GASFLOW-MPI analysis on deflagration in full-scale hydrogen refueling station experiments: H_2-air premixed cloud and high-pressure H_2 jet

Fangnian Wang[*], *Jianjun Xiao*[**], *Thomas Jordan*

Institute of Thermal Energy Technology and Safety (ITES), Germany Karlsruhe Institute of Technology (KIT), Germany

ARTICLE INFO

Keywords:
Hydrogen deflagration
Premixed cloud
High-pressure jet
GASFLOW-MPI
Hydrogen refueling station

ABSTRACT

Safety of the hydrogen refueling station under a postulated accident (e.g. leakage) is of great importance in hydrogen energy. The predictive CFD tool GASFLOW-MPI is utilized to simulate the full-scale hydrogen refueling station deflagration experiments with premixed H_2-air cloud and high-pressure H_2 jet. The overpressures are predicted for an ignition between two dispensers in the premixed trial and a spark in the engine bay in the jet trial, which agree with the experimental data and validate the GASFLOW-MPI as well. Five turbulent burning velocity models are involved to investigate the explosion of the premixed H_2—air cloud. The Zimont correlation is recommended for the combustion simulation of engineering full-scale H_2 refueling station. The turbulent flame speed is predicted after an ignition resulting in 50–200 m/s, and the flame acceleration happens due to the turbulence effect by obstacles. The developments of the pressure, temperature and H_2 concentration of premixed H_2-air deflagration, indicate the pressure wave propagates with the reflections on obstacles, and the flammable H_2 cloud is enlarged by the push of combustion product.

Moreover, the standard $k-\varepsilon$ and DES model are adopted on the jet dispersion analysis. The local flow variables show some differences, but the global properties of average hydrogen concentration, the shape and size of the burnable cloud are similar, which indicates the hydrogen dispersion transient computed by $k-\varepsilon$ turbulence model provides a reliable basis for estimating the combustion process. The evolutions of the jet resulting burnable H_2-air mixture in the domain in terms of H_2 velocity field, concentration and mass are evaluated. The velocity field in jet trial explains that the momentum dominates hydrogen dispersion and result in a corresponding hydrogen concentration, however a large zone with high turbulence forms after combustion. The analysis of H_2 dispersed in the engine bay shows the growth and decay of the hydrogen concentration above some

* *Corresponding author.*
** *Corresponding author.*
E-mail addresses: fangnian.wang@kit.edu (F. Wang), jianjun.xiao@kit.edu (J. Xiao).

specified value of interest (4 and 10 vol% H_2). Most dispersed H_2 cloud is burnable, and half of the mass distributed in the cloud above 10 vol% may accelerate the flame to sonic. The comparison of the overpressure in $k-\varepsilon$ and DES turbulence models with real and ideal gas release sources, shows in general no significant difference. The hydrogen release jet with higher turbulence generates the hydrogen cloud that can result in a large overpressure.

Introduction

A potential solution to reduce greenhouse gas emissions is to use vehicles powered by hydrogen produced from renewable energy [17], like solar power. We call it solar hydrogen in our present project. Widespread adoption of these vehicles would require plenty of hydrogen refueling stations. Hydrogen has been safely managed burnable gas for many years, but in the environment of a hydrogen refueling station, the normal safety understanding would be inappropriate. In the refueling station, the public is allowed to handle high-pressure (40/70 MPa) hydrogen during the refueling process. Therefore, the hazards of the hydrogen use in hydrogen refueling stations should be noticeable. The hydrogen explosion accident happened in Norway gave us the importance of hydrogen safety [13]. It is essential to understand the hazards caused by an accidental hydrogen leakage and develop the appropriate tools (codes) to predict the consequence of accidents.

The predictive tools for hydrogen safety engineering, such as computational fluid dynamics (CFD) codes CFX, FLUENT, OpenFOAM and GASFLOW-MPI etc., are essential for the design of safe hydrogen applications [11]. GASFLOW-MPI is the advanced parallel version of the GASFLOW sequential code with many newly developed and validated models and features. GASFLOW-MPI has been well verified and validated by many international benchmarks on shock wave, premixed/nonpremixed turbulent combustion, detonation in tubes etc., which reveals the reliability in predicting all speed flow-fields associated with hydrogen safety coupling heat and mass transfer [28,31].

Nevertheless, there is still room for the further validation of GASFLOW-MPI utilizing in the real scale and open zone of hydrogen refueling station, and the investigation of the suitable physical models for the simulations, e.g. the turbulence model and combustion model for the simulation of hydrogen dispersion and explosion, even the model of high-pressure hydrogen release. Accordingly, the implemented combustion models and turbulence models in GASFLOW-MPI should be assessed in the simulation of the accidental hydrogen explosion in a full-scale refueling station, and demonstrate further the credibility and the performance level of the code, and consequently figure out the effects of the combustion and turbulence models.

Turbulent burning velocity correlations are wildly used in the CFD simulation of combustion of premixed burnable gas (including hydrogen). E.g. Zimont correlation has been developed based on a theory of premixed combustion with high Reynolds number [34]. The correlation depends on the physico-chemical properties of the combustible mixtures and turbulence parameters. The constant in the model is around 0.5 for H_2-air mixtures recommended by zimont's validation work. Zimont correlation was implemented in CFD tools, such as CFX, GASFLOW-MPI, FLUENT, OpenFOAM and validated against hydrogen deflagration experiments [6,7,15,27]. These CFD calculations coupling Zimont correlation with minor adjustment of the scaling factor agree well with the experimental data, which reveals it is reliable to model the turbulent burning velocity. However, Zimont model evaluates flame propagation of completely developed turbulent flames. Laminar flame propagation and transition from laminar flames to turbulent flames are not accounted for. The further summary of the literature study of five turbulent burning velocity models, i.e. Zimont and Mesheriakov, Zur Loye and Bracco, Peters, Schmid, Zimont models, and two turbulence models, i.e. k ε and Detached Eddy Simulation (DES) models, are presented in Section 2 Mathematical model.

With respect to the large scale hydrogen explosion experiments for validation, Sandia National Laboratories [19] carried out a series of large scale experiments on flame acceleration (FA) and deflagration to detonation transition (DDT) for H_2-air mixture in a rectangular channel with obstacles, indicated that the presence of the obstacles greatly increased the flame speed and the potential of DDT [23]. Conducted the explosion experiments of high-pressure hydrogen (40 MPa) leakage in a hydrogen refueling station, which indicated that explosion overpressure was strongly dependent on the turbulent flow of leakage. Tanaka et al. [24] studied homogeneous H_2-air mixtures explosions in a full-scale hydrogen refueling station model experimentally, which shown the hydrogen concentration dominate the flame speed and overpressure Shirvill et al. [20,21] carried out experiment series of the deflagration of H_2-air premixed cloud and high-pressure H_2 jet in a full-scale refueling station, and investigated the explosion overpressure evolutions. These previous experiments provide useful insights and database to develop and validate the CFD codes applying for the hydrogen refueling stations. After the literature review, we find the Shirvill's full-scale experiments published relatively complete experimental data covering wide range, which are quite useful for our current investigations.

The objectives of the present paper are therefore to:

- validate the GASFLOW-MPI modelling using the H_2 deflagration experiments of premixed cloud and high-pressure jet in a full-scale refueling station.
- investigate flame development and propagation, the high-pressure H_2 release and dispersion with the effects of combustion models and turbulence models.

The paper is structured as follows: the key physical models involved in the present simulations and analyses are presented in the mathematical model section; the GASFLOW-MPI modelling section describes the introduction of the experiments used for the validation, and the role of GASFLOW-MPI modelling in hydrogen deflagration analyses, including the applied mesh, initial and boundary conditions. Followed by the description of numerical model, the simulation results and discussions are presented, including the code validation, the investigation on combustion model, turbulence model on flame propagation and the high-pressure H_2 release, dispersion and combustion. The summary and conclusions are then presented in the last section.

Mathematical model

GASFLOW-MPI is a parallel finite-volume CFD code that adopts the Implicit Continuous Eulerian - Arbitrary Lagrangian Eulerian (ICE'd-ALE) solution algorithm [28–30]. GASFLOW-MPI is applicable to all speed flows from incompressible to supersonic flow regimes, which is allowed to simulate major hydrogen safety related phenomena, such as release, turbulent dispersion, deflagration and detonation. In this section, we will only concentrate on the combustion models and the RANS/DES based turbulence models.

- Combustion model

In order to model the flame front propagation, the transport equation of the density-weighted mean reaction progress variable, ξ, is solved [29]:

$$\frac{\partial}{\partial t}(\rho\xi) + \nabla\cdot(\rho\xi\boldsymbol{u}) = \nabla\cdot\left[\left(\rho\alpha_u + \frac{\mu_t}{Sc_t}\right)\nabla\xi\right] + \rho S_\xi \tag{1}$$

where ρ is the density, $\boldsymbol{u}$ is the velocity, t is the time, α_u is the thermal diffusivity of the unburned mixture, μ_t is the turbulent dynamic viscosity, Sc_t is the turbulent Schmidt number. For hydrogen fueled mixtures, the mean combustion progress variable, ξ, is usually written as:

$$\xi(\boldsymbol{x},t) = \frac{Y_{H_2,unburnt}(\boldsymbol{x},t) \quad Y_{H_2}(\boldsymbol{x},t)}{Y_{H_2,unburnt}(\boldsymbol{x},t) \quad Y_{H_2,burnt}(\boldsymbol{x},t)} \tag{2}$$

where $\boldsymbol{x}$ the position vector, Y represents the local mass fraction of the species. $Y_{H_2,unburnt}$ and $Y_{H_2,burnt}$ are the hydrogen mass fraction in the zones of unburnt reactants and fully burnt products, respectively. Obviously, the progress variable, $\xi = 1$ in the burnt mixture and $\xi = 0$ in the unburnt mixture.

The key of this modelling approach is the method of solving the source term, ρS_ξ. Actually GASFLOW-MPI provides various concepts to model this source term with their own specific assumptions, e.g. the Arrhenius rate model neglecting the turbulence effect, and the eddy dissipation model assuming the combustion occurs at small scale where the fuel and oxidizer mix on the molecular scale with sufficiently high temperature [10]. The method based on progress variable gradient would be better for the present problem – deflagration in the full-scale hydrogen refueling station, in order to evaluate the correlations additionally. The source term of the mean reaction progress can be modelled as:

$$\rho S_\xi = \rho_u S_T |\nabla\xi| \tag{3}$$

where ρ_u is the density of unburnt mixture, and S_T is the turbulent flame speed. The key of implementing this approach is to find a suitable correlation of S_T. GASFLOW-MPI currently provides several correlations for turbulent flame speed, as show in Table 1. Dozens of correlations as shown in reference [4] could be tested in calculation, if the already implemented correlations are not sufficient.

The parameters in the turbulent flame speed model are listed as follows:

- Laminar flame speed S_L

The laminar flame speed S_L is a physical-chemical property of the mixture and thermodynamic conditions (pressure and temperature) upon mixture ignition. Here, the correlation from Refs. [1,2] considering the effect of diluent is used for the H_2-air-H_2O mixture:

$$S_{L,ref} = (1.44\phi^2 + 1.07\phi \quad 0.29)(1 \quad \varphi)^4 \tag{9}$$

where ϕ denotes the equivalence ratio, φ is the diluents (e.g. steam, He, CO_2 etc.) volume fraction, and $S_{L,ref}$ laminar flame speed at the reference pressure $P_{ref} = 103125$ Pa and temperature $T_{ref} = 298$ K.

The compression of unburned gas ahead of the flame may increase the pressure and temperature. Taking the effects of compression into account, the thermo-dynamic correlation of the laminar flame speed S_L can be expressed [12] with the exponents of hydrogen:

$$S_L = S_{L,ref}\left(\frac{P_u}{P_{ref}}\right)^{0.26}\left(\frac{T_u}{T_{ref}}\right)^{(1.524+0.026\phi)} \tag{10}$$

where P_u and T_u are the pressure and temperature of the unburned mixture respectively. The thermal diffusivity of the unburned gas is modified in terms of pressure and temperature as well:

$$\alpha_u = \alpha_{u,0}\left(\frac{P_u}{P_{u,0}}\right)^{\phi}\left(\frac{T_u}{T_{u,0}}\right)^{\lambda} \tag{11}$$

where $P_{u,0}$, $T_{u,0}$ and $\alpha_{u,0}$ are the initial pressure, temperature and thermal diffusivity of the unburned mixture, respectively.

- Turbulence dependent parameters

The integral turbulent velocity fluctuation $u_t' = \sqrt{\frac{2}{3}\kappa}$, where the κ is the turbulent kinetic energy.

Damköhler number, Da, is defined as the ratio of the turbulent integral time scale τ_t to the chemical time scale τ_c:

$$Da = \frac{\tau_t}{\tau_c} \tag{12}$$

where the turbulent integral time scale, $\tau_t = \frac{l_t}{u_t'}$, where the integral length scale l_t is associated with the turbulence; and the chemical time scale is defined as $\tau_c = \frac{\alpha}{S_L^2}$, where α is the

Table 1 – Correlations of turbulent flame speed.

Reference	Correlation
[36]	$S_T \quad S_L\left[1+1.25\left(\frac{u_t'}{S_L}\right)^{0.7}\right]$ Eq. 4
[33]	$S_T \quad (u_t')^{0.75}Da^{0.25}$ Eq. 5
[22]	$S_T \quad S_L + u_t'\left(\frac{Da^2}{1+Da^2}\right)^{-0.25}$ Eq. 6
[14]	$S_T \quad S_L\left\{1-0.195\frac{l_t}{l_F}+\left[\left(0.195\frac{l_t}{l_F}\right)^2+0.78\frac{u_t'}{S_L}\frac{l_t}{l_F}\right]^{0.5}\right\}$ Eq. 7
[34]	$S_T \quad 0.52(u_t')Da^{0.25}$ Eq. 8

thermal diffusivity of gas. The flame thickness, l_F is therefore defined as:

$$l_F = \frac{\alpha}{S_L} \tag{13}$$

- Turbulence model

Since the numerical simulations are based on the solution of fully compressible Navier-Stokes equations, and the combustion model is dependent on the turbulent kinetic energy κ and the turbulent dissipation rate ε. The combustion model in GASFLOW-MPI has been coupled with RANS-based turbulence $k \quad \varepsilon$ model and Detached Eddy Simulation (DES) model. The well-known $\kappa \quad \varepsilon$ model [9] is a two equation model that gives a general description of turbulence by means of two transport equations in terms of the transported variables κ and ε :

$$\frac{\partial(\rho\kappa)}{\partial t} + \nabla\cdot(\rho\kappa\mathbf{u}) = \nabla\cdot\left[\left(\mu+\frac{\mu_t}{\sigma_\kappa}\right)\nabla\kappa\right] + P_\kappa + P_{\kappa b} \quad \rho\varepsilon \tag{14}$$

$$\frac{\partial(\rho\varepsilon)}{\partial t} + \nabla\cdot(\rho\varepsilon\mathbf{u}) = \nabla\cdot\left[\left(\mu+\frac{\mu_t}{\sigma_\varepsilon}\right)\nabla\varepsilon\right] + C_{\varepsilon 1}\frac{\varepsilon}{\kappa}(P_\kappa + P_{\kappa b}) \quad C_{\varepsilon 2}\rho\frac{\varepsilon^2}{\kappa} \tag{15}$$

where μ is the dynamic viscosity, and μ_t is the turbulent viscosity that can be written as:

$$\mu_t = \frac{C_\mu \rho \kappa^{1/2}}{\varepsilon} \tag{16}$$

The turbulence generation due to the viscous forces, P_κ, is calculated as:

$$P_\kappa = \quad \frac{2}{3}\rho\kappa\nabla\cdot\mathbf{u} \quad \frac{2}{3}\mu_t(\nabla\cdot\mathbf{u})^2 + \mu_t\nabla\mathbf{u}\cdot\left[\nabla\mathbf{u}+(\nabla\mathbf{u})^T\right] \tag{17}$$

The turbulence production term due to the buoyancy, $P_{\kappa b}$, is computed as:

$$P_{\kappa b} = \quad \frac{\mu_t}{\sigma_b}\mathbf{g}\cdot\nabla\rho \tag{18}$$

where the constant coefficient, σ_b, is 0.7 and $\mathbf{g}$ is the gravitational acceleration.

DES turbulence model used in the present simulation is a hybrid RANS/LES turbulence model. Compared with the pure RANS model, the DES model could capture more detailed turbulent information in the small-scale region. Meanwhile, for the large-scale region, the DES model could use relatively coarse mesh, where the RANS model is adaptively employed to reduce the computational cost. Different from the original standard $k \quad \varepsilon$ model, the turbulence length scale in DES turbulence model coupled in the two turbulence transport equations is the minimum between the standard $k \quad \varepsilon$ model and the LES model [35], as shown following:

$$l_t = min\left(C_\mu\frac{\kappa^{3/2}}{\varepsilon},\ C_{DES}\Delta_{max}\right) \tag{19}$$

where Δ_{max} is the maximum of the filter cut-off scale, which is obtained from the box filter over grid cells in x, y, z three coordinates. When the mesh size is fine enough, the LES model is employed, so that the detailed turbulent fluctuation behavior could be captured. For the large mesh size region, the DES model is equivalent to the standard $k \quad \varepsilon$ model. The values of the constant coefficients in the $k \quad \varepsilon$ model and DES model are listed in the nomenclature.

- High-pressure H_2 release model

The hydrogen release is important for simulating the high-pressure hydrogen leakage in a refueling station. The release rate was modelled in GASFLOW-MPI by assuming a choked flow (or sonic release) from the high-pressure H_2 storage through an orifice when the ambient pressure is much smaller (at least 0.5266 times) than the pressure in storage, or modelled by a subcritical flow. For an ideal gas, the release rate is of the form:

$$\dot{m} = AC_d\begin{cases}\sqrt{\gamma p_1\rho_1\left(\frac{2}{\gamma+1}\right)^{\frac{\gamma+1}{\gamma-1}}}, & \frac{p_2}{p_1} < \left(\frac{2}{\gamma+1}\right)^{\frac{\gamma}{\gamma-1}} \\ \sqrt{2p_1\rho_1\frac{\gamma}{\gamma \quad 1}\left[\left(\frac{p_2}{p_1}\right)^{\frac{2}{\gamma}} \quad \left(\frac{p_2}{p_1}\right)^{\frac{\gamma+1}{\gamma}}\right]}, & \frac{p_2}{p_1} \geq \left(\frac{2}{\gamma+1}\right)^{\frac{\gamma}{\gamma-1}}\end{cases} \tag{20}$$

where $\dot{m}$ is the mass flow rate through the orifice/hole with cross-section area A and user estimated discharge coefficient C_d, normally 0.9–0.97. The ratio of specific heats at constant pressure and constant volume, $\gamma = \frac{C_p}{C_v} = 1.41$. The relevant static pressures on either side of the orifice/hole, with p_1 and ρ_1 corresponding to the high pressure and gas density, with p_2 and ρ_2 corresponding to the low pressure and gas density, respectively, are specified.

Concerning the high-pressure release to the ambient pressure 1 bar, the mass release rate can be modelled as choked flow of quite long duration (tens of seconds), which lasts until the ratio of the storage pressure over the ambient

pressure equals 1.9. Substituting the ideal gas low and solving the first order ordinary differential equation as below:

$$\dot{m}(t) = AC_d\sqrt{\gamma p(t)\rho(t)\left(\frac{2}{\gamma+1}\right)^{\frac{\gamma+1}{\gamma-1}}} = V\frac{d\rho}{dt} \tag{21}$$

$$\dot{m}(t) = \dot{m}_0 exp\left(C_d\frac{A}{V}t\sqrt{\gamma R_{H_2}T\left(\frac{2}{\gamma+1}\right)^{\frac{\gamma+1}{\gamma-1}}}\right) \tag{22}$$

where $\dot{m}_0$ is the initial release mass flow rate with the initial pressure and density in a high-pressure hydrogen storage tank, V is the volume of the storage tank. R_{H_2} is the gas constant for hydrogen, 4124.24 J/(kg·K), T is the temperature. The ideal gas release mass flow rate over time decreases exponentially that is consistent with the result in Ref. [5].

GASFLOW-MPI modelling

Experiment layout

As we discussed in the introductory section, the full-scale experiments with premixed hydrogen-air cloud and high-pressure jet conducted by Health and Safety Laboratory, UK [20,21], are selected to be simulated in present work. The experiments were offered as a standard benchmark of explosion in a realistic refueling station. The experimental rig (4.2 m high, 0.6 m wide and 5.4 m long) consisted of a dummy vehicle, two dispenser units and a concrete confining wall. Two dispensers were made of steel standing on the concrete pad. The vehicle and dispenser were made of steel plates with thickness 8 mm. The engine bay of the vehicle was open from the bottom to allow it to be filled with a hydrogen–air mixture. The pressure sensors and ignition position for premixed and jet trials, as described in the Supplementary Data Fig. S1. The pressure monitor points of both trials are quite similar. The transducers were mounted on the dispenser and on the confining wall at different heights, under the vehicle, and across and along the vehicle as well. The pressure recorded are used in the comparison with simulated pressure dynamics.

Actually, there are 4 tests with different ignition locations in the premixed trial, and 3 tests with different jet duration in the jet trial. In the present simulation, we selected one test with more experimental data published of each trial. The initial and boundary conditions of the typical test in premixed trial and jet trial respectively are: In the premixed trial, the total volume of the hydrogen–air mixture was 70.16 m^3 (2.5 m high, 0.6 m wide and 5.4 m long frame excluding the volume of sealed dispensers and mock-up vehicle) with the mass of hydrogen ignited 1.847 kg and 31.4 vol% H_2 contained in the plastic film frame. The gas mixture temperature at the ignition moment was 302 K, and relative humidity 42.1%. The ignition source was located between the dispensers 1.3 m from the confining wall and 1.25 m above the ground. In the jet trial, the hydrogen leakage released vertically downwards 1.2 m above the ground. The release nozzle was connected to the hydrogen storage cylinder with a 12 m long, 15 mm inner diameter flexible hose. Time of spark started after release is 0.7 s. The initial vessel density and mass flow rate were 26.69 kg/m^3 and 1.02 kg/s, while the density and mass flow rate at the moment of ignition were 24.37 kg/m^3 and 0.913 kg/s with pressure 35.53 MPa and temperature 286.8 K in the vessel. The hydrogen mass release at ignition time was 0.675 kg. However, two kinds of mass fraction of the hydrogen release (ideal gas and real gas) are involved in present calculation. We take the ideal gas release as the injection boundary, meanwhile compare the case of real gas release in the discussion section (More experiment details can be seen in Refs. [11,21].

GASFLOW-MPI modelling set-up

The geometry model is drawn by the AutoCAD exporting as a *.stl file, which can be pre-processed via the tool Pyscan to convert to cartesian structured mesh, as shown in Fig. 1. The mesh domain size is 34.4 m (x-direction) X 44.8 m (y-direction) X 22.4 m (z-direction) with the cell resolution $144 \times 123 \times 76 \approx$ 1,3 million. The core of the calculation part (namely, the zone of the experiment) meshes as cubic cells with the cell length $\Delta x = 10\ cm$. A coarse mesh with $\Delta x = 20\ cm$ is also applied for the mesh resolution dependency. The mesh size of the mock-up refueling station is acceptable by many CFD activities in Refs. [11,26]. In the present study the coarse mesh is applied in the premixed trial, while the fine mesh is used in the jet trial due to the high turbulence of the jet. Each boundary of both mesh has several 'stretched' additional meshes for dissipating the pressure wave reflection.

A non-slip boundary condition is applied to the walls of all the components of the facility. The standard $k \quad \varepsilon$ turbulence model coupling wall functions and Zimont turbulent flame model are adopted. The pressure iteration convergence tolerance is 10^{-6}. Regarding problem time (< 2 s) and space discretization, the well-known second order accuracy Van Leer scheme has been employed for the discretization of the convective terms. An automatic time step increase/decrease mechanism has been applied with a 10^{-5} s as initial time step. The time step has been restricted by a maximum permitted time step of 10^{-4} s, which corresponds to a maximum Courant–Friedrichs–Lewy (CFL) number of 0.25. The CFL number can be relaxed to nearly 1. The value 0.25 in present calculation is recommended mainly for accuracy.

The geometry slightly differs from these two trials. In the jet trial, the dispensers are slightly displaced towards the vehicle. Meanwhile, the 'engine bay' section is hollow and only open at the bottom face (see the corresponding hollow space inside the walls around the 'engine bay' in Fig. 1) while the 'passenger' section is closed on all side walls. The ignition in the simulation is initiated as a high temperature cell (1800 K) within a short time duration (10^{-5} s).

Result and discussion

Simulations with conditions in a matrix (2 turbulence models X 5 turbulent flame speed correlations) are conducted. The following validation part addresses the simulated predictions compared with experimental data by the best models

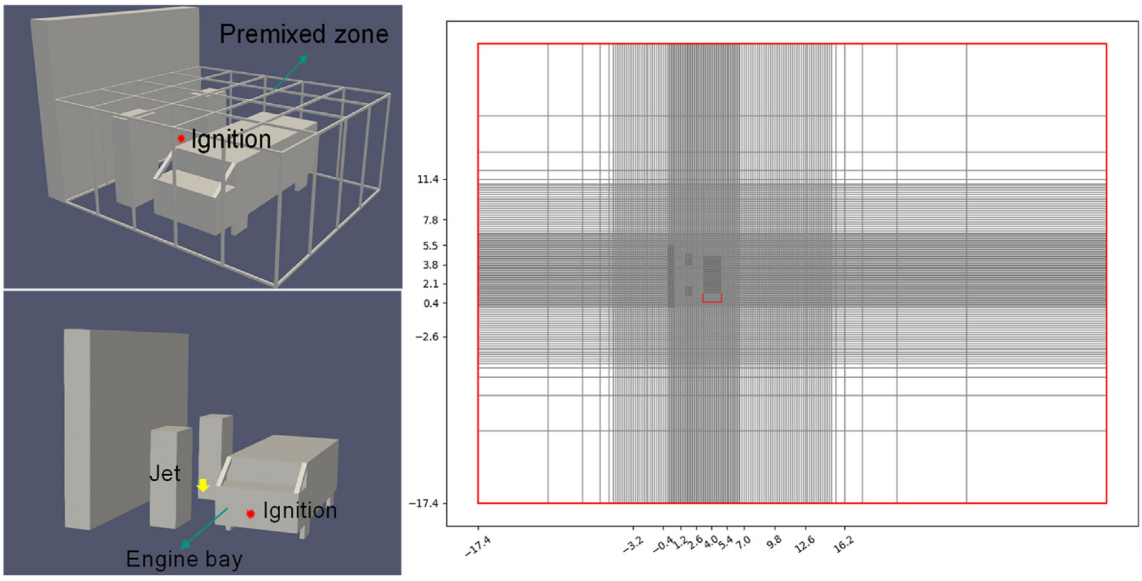

Fig. 1 – Mesh ($\Delta x = 10\ cm$, x-y plane at elevation 0.5 m) and view of GASFLOW-MPI modelling.

identified. The discussion part presents the propagation of premixed flame and the high-pressure jet dispersion and combustion.

Results comparing with experimental data

- Premixed trial

The experimental data [20,21] provided overpressure dynamics for the comparison. The comparison as far as possible between the simulated pressure evolutions and the experimental data extracted by digitizing the published results at each transducer (i.e. KD1, K2, K3, K4, K5, K6, KW7, K10, KW12, KW13, KW14, H15, H16, there are no other published data) is given in Fig. 2 with the corresponding subfigures respectively.

The smoothed overpressure traces, no matter for transducers under the vehicle or close to the confined wall and dispensers, are predicted well in general, as shown in Fig. 2. The pressure increases moderately and the peak (or two peaks in some locations K2, K3, K4 under the vehicle) of overpressure occurs after the ignition. The positive impulse lasts 20–40 ms, then the impulse goes to negative. The comparisons show good predictions generally. The monitor points mounted on the wall (e.g. KW7) have larger deviation since the comparing calculation results is extracted from the first cell layer that is 20 cm far away from the wall.

From Fig. 2, the maximum explosion overpressures are relatively larger and earlier under the vehicle than the other place due to the congestion and the resulting flame acceleration. Furthermore, the maximum overpressures of the sensors across and along the vehicle is illustrated in Fig. 3. The horizontal maximum overpressures across the vehicle decrease over the distance, also the vertical maximum overpressures along the vehicle decrease over the distance from both sides of the vehicle center. The calculation results are comparable with the experimental data.

- Jet trial

The high-pressure hydrogen mass release in this trial is 0.675 kg before the sparking. However, the experiment didn't indicate the mass flow rate over time. Two kinds of mass fraction of the hydrogen release (ideal gas and real gas) are involved in present calculation. We have confirmed that the initial mass flow rate ($\dot{m}_0 = 1.01\ kg/s$) in the experiment is consistent to the result calculated via Eq. (20). Therefore, we take the ideal gas release as the injection boundary, meanwhile compare the case of real gas release in the later discussion section.

Similar to the premixed trial, the experimental data of jet trial from Ref. [20] offers the overpressure dynamics at different locations. The comparisons between the predictions and experimental data at each pressure transducer (i.e. S1, S2, S3, S4, S5, S7, S9, S10, S14, the other transducers' data are not published or in the very far field with very low overpressure) are given respectively in Fig. 4 subfigures. The sensors 1, 2 and 3 are under the vehicle where the sensor 3 being right under the sparking location. The sensors 4, 5, 7 and 9 are mounted on the wall and dispenser at various elevations while the sensors 10, 14 are located in the near field outside the vehicle.

Different from the premixed case, as shown in Fig. 4, the pressure increases rapidly and reaches the peak very soon after the ignition since the turbulence kinetic energy has already been set up due to the high turbulent combustion velocity caused by the high-pressure jet release before sparking. The positive impulse lasts a short period and then goes to negative. It can be seen in Fig. 4 that the predictions have captured the trend of the measured overpressure developments well, however, the discrepancies in the comparison are still obvious. The jet trial involves many complicated phenomena such as jet release, dispersion and the wind effect etc., which could cause uncertainties in simulations.

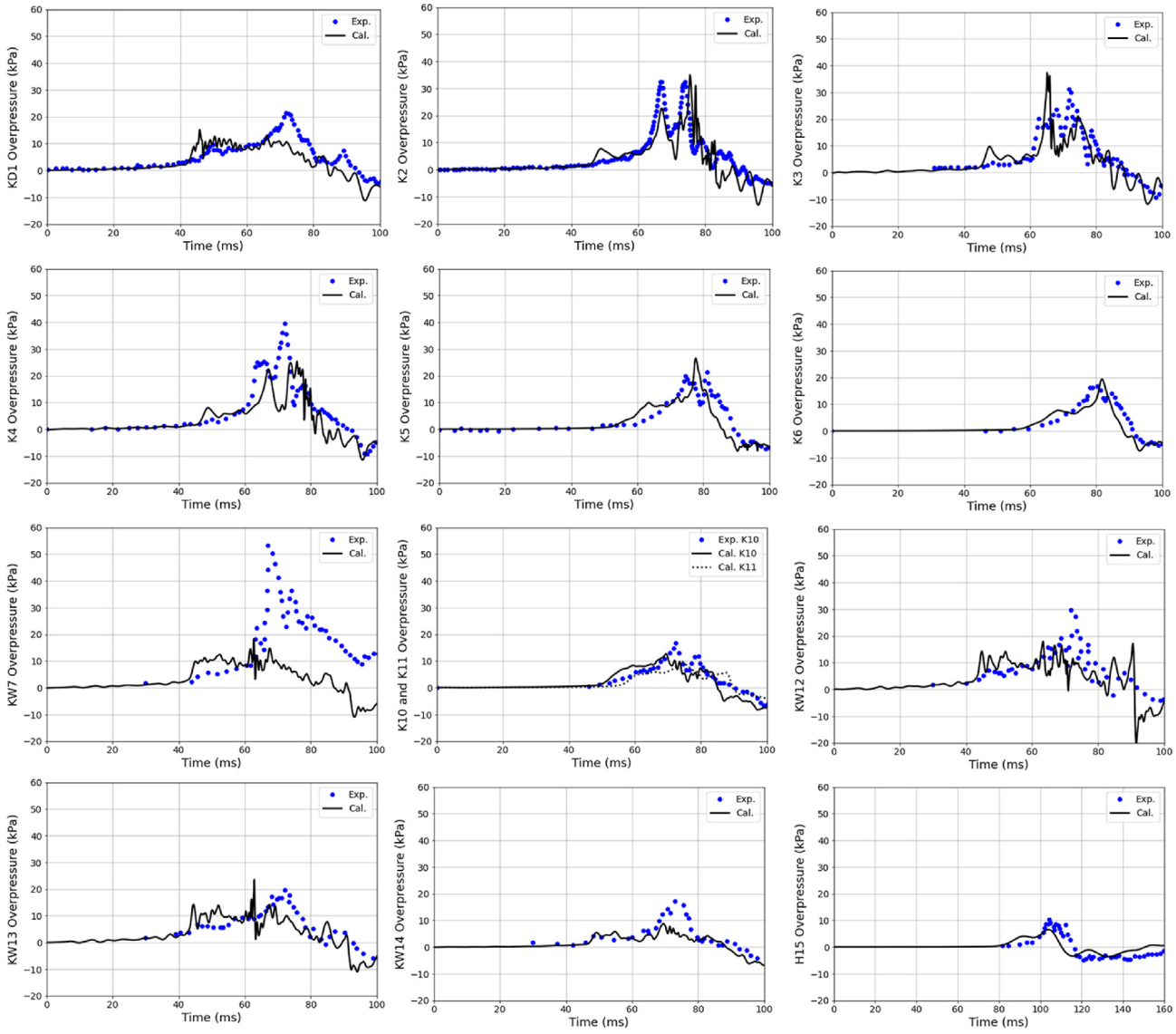

Fig. 2 – Overpressure evolution of each sensors in premixed trial.

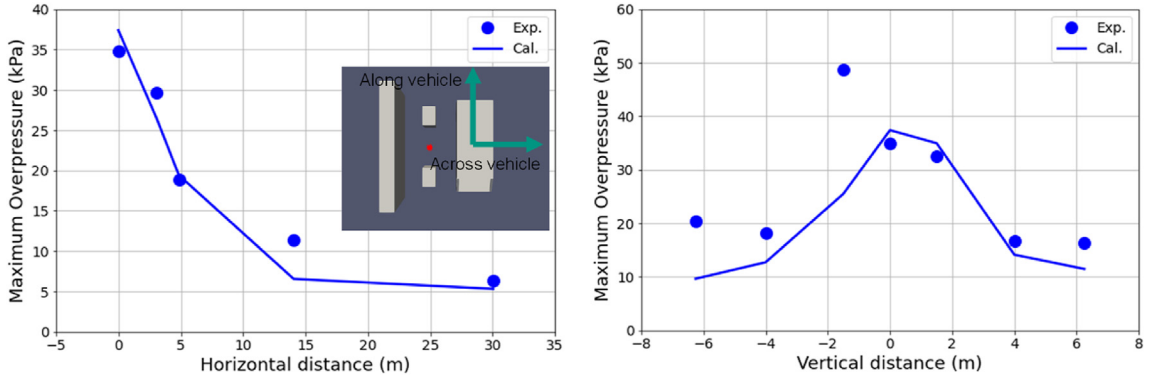

Fig. 3 – Maximum overpressure across and along the vehicle in premixed trial (note: horizontal distance means the sensors' displacement across the vehicle from the vehicle center, while the vertical distance is the displacement along the vehicle from the vehicle center).

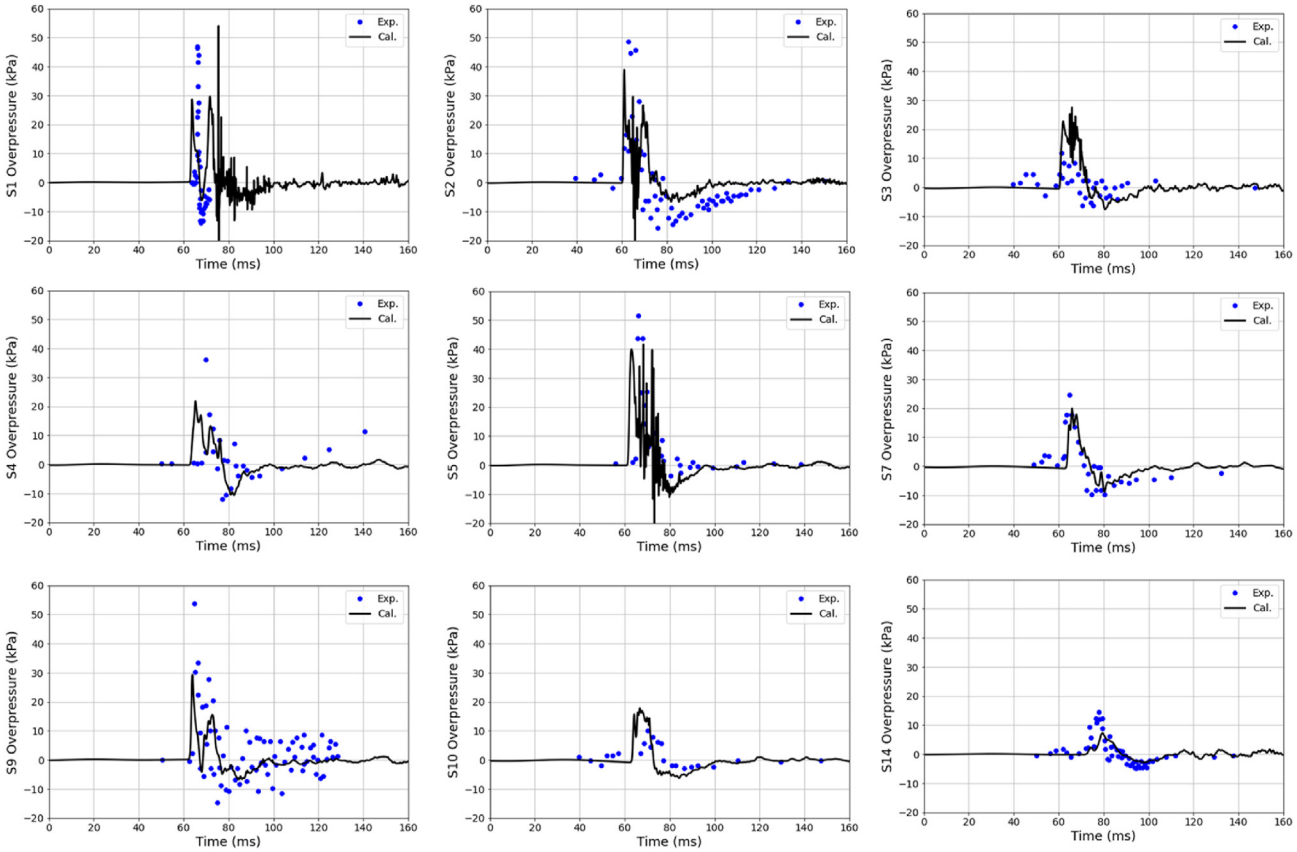

Fig. 4 – Overpressure evolution of each sensor in jet trial.

The comparison between the predictions and measurements of maximum overpressure are summarized in Supplementary Data Tab. S1. Similar to the premixed case, the maximum overpressures decays over the distance across and along the vehicle. The differences between the predicted and measured overpressures are significant (Relative Error = 20–90%). The peaks of the overpressures under the vehicle are higher than outside vehicle due to the higher hydrogen concentration and flame acceleration in the confinement.

The above comparisons of both premixed and jet trials on overpressure evolutions and maximum overpressures generally are consistent with the experimental data, even though there are some reasonable deviations at some specific sensor locations. As a short summary, the physical phenomena contributing to overpressure dynamics and maximum overpressures in both trials in principle are modelled well by GASFLOW-MPI with the current modelling set-up. Namely, the presently used mesh ($\Delta x = 10$ cm for real scale case), combustion model (Zimont model) and turbulence model (standard $k \quad \varepsilon$ model) are acceptable for the further analysis of the full-scale hydrogen refueling station.

Discussion

- Flame propagation

GASFLOW-MPI provides the combustion module to model the dynamics of turbulent flame propagation. Here, in order to obtain the flame front propagation, the transport equation of the density-weighted mean reaction progress variable coupling the turbulent flow model is solved. For the possible combustion regimes of slow laminar deflagration, fast turbulent deflagration, and fully developed detonation, the typical flame speeds and resulting unreflected overpressures roughly vary from 2 to 2000 m/s, and from 0.01 to 10 bar of magnitude [3]. The prediction of the combustion regime is actually strongly influenced by the turbulent burning velocity, which is dominated by the turbulent fluctuation u_t' and the Damköhler number Da, etc., like expressing as a dimensionless form $\frac{S_T}{S_L} = f\left(\frac{u_t'}{S_L}, Da, \ldots\right)$.

With five different turbulent flame speed correlations, as shown in Table 1 respectively, the flame speed and the resulting overpressures are computed in present simulations. We take the comparisons of each representative overpressure under the vehicle, close to the wall, across and along the vehicle in the premixed trial as examples to present the sensitivity analysis on turbulent flame speed. Fig. 5 indicates the predictions with these five turbulent burning velocity correlations enclose the experimental data and have similar trends. The comparisons of the other locations' overpressure are quite similar to those representatives qualitatively (as seen in Supplementary Data Fig. S2). The predictions by Peters' and Schmid's models are higher, while those by Zimont's and Zur Loye's models are closer and the one by the Zimont and Mesheriakov's model is lower than the experimental data. The applied empirical correlations have their own limitations (e.g.

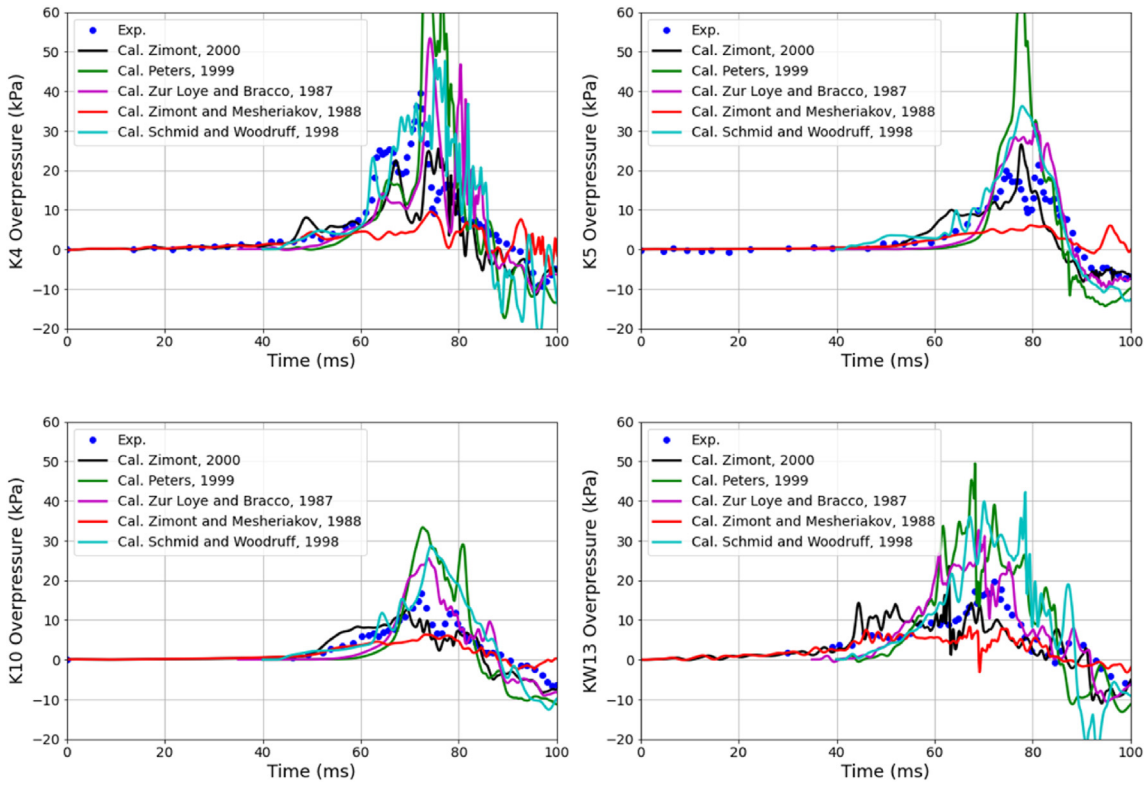

Fig. 5 – Overpressures in premixed trial with different turbulent burning velocity correlations: K4 under vehicle, K5 across vehicle, K10 along vehicle, KW13 on the wall.

the range of Reynolds numbers) and turbulence-dependent, e.g. the Zimont [34] model has a large exponent of turbulence fluctuation and is valid at high *Re* and *Da* numbers. According to the present results, the Zimont model is acceptable for the current conditions – engineering full-scale H_2 refueling station, which is also the default turbulent flame speed correlation (if the reaction progress variable combustion concept is triggered) in GASFLOW-MPI.

The left subfigure in Fig. 6 shows the temperature dynamics (simulated with Zimont [34] correlation and $k \quad \varepsilon$ turbulence model) at different locations in the burnable cloud of the premixed trial. The locations are gradually getting farther away from the spark. Each temperature increases very sharply at some point of time, since the flame front has propagated there. As a result, the average flame velocity can be approximated by the known flame propagation distance and the time duration. There is a large temperature gradient at the flame front, since it is an intuitive consequence of the hydrogen combustion. The temperature in the unburnt zone is the room temperature, while it is over 1000 K in the burnt zone. Let's choose 1000 K artificially as a temperature reference to find the time duration between each two neighboring points. The estimated average flame speed across the vehicle is shown in the right subfigure of Fig. 6. It is very clear that the flame velocity near the ignition is quite low but increases rapidly over the distance, and decreases after reaching the peak. The flame

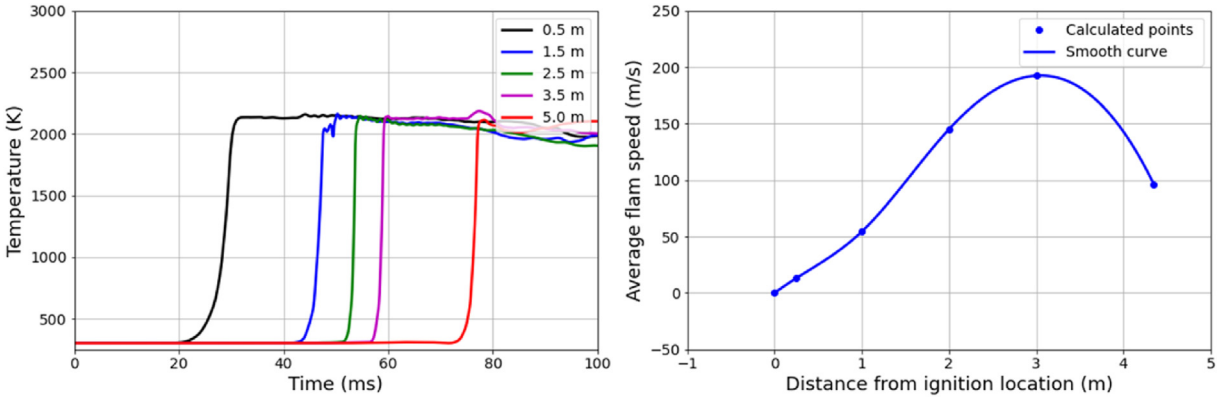

Fig. 6 – Temperature across the vehicle at various distances apart the ignition location (left), the estimated average flame speed across the vehicle (right).

acceleration is due to the obstacle of the mock-up vehicle enhancing the effect of turbulence. The importance of the turbulent burning velocity model is confirmed again here. Using fixed burning velocity, such as some calculations in Ref. [11], is not accurate enough, however, if the maximum burning velocity is adopted as the fixed value, with respect to the safety the conservative consequence will be obtained.

Fig. 7 (upper row) illustrates the sequenced snapshots corresponding to the pressure field of premixed H_2-air deflagration (simulated with Zimont correlation and $k \quad \varepsilon$ turbulence model). The pressure fields at 30 ms, 60 ms, 90 ms after ignition, indicate the pressure wave propagation in the space with the reflections from the obstacles, namely the two dispensers, mock-up vehicle and the walls. Fig. 7 (middle and lower row) illustrates temperature field and volume fraction of H_2 development respectively at the same time. The range of the color bars are fixed in [1, 1.1] bar of pressure, [0, 2500] K of temperature, and [0, 32] % of H_2 volume fraction. From these figures, we find that: 1, the temperature and H_2 volume fraction propagation are consistent with the subsonic flame speed we discussed above, however the pressure wave propagates faster. 2, the boundary of the temperature front where the temperature gradient varies rapidly, almost overlaps the H_2 volume fraction front which indicates the flame front propagation. 3, the flammable H_2 cloud at the beginning is the premixed H_2 zone, however, its size increases during the H_2 combustion, since the combustion product pushes the unburned high concentration H_2 away into the lean/non H_2 space. 4, it doesn't always have a detonation in a premixed cloud with high concentration of hydrogen (32 vol%) if the cloud is (almost) stagnant or initial turbulence is not high enough.

- High-pressure jet release, dispersion and combustion

High-pressure hydrogen leak from a tank is quite often discussed as a postulated accident in a hydrogen refueling station. In our previous work [3], GASFLOW-MPI was used to investigate a similar scenario involves supersonic hydrogen release and turbulent dispersion from a pressurized reservoir into a room, followed by an accidental ignition of the resulting H_2-air cloud. In the present jet trial, the supersonic jet at the release location is expected. We apply the pre-expended method (e.g. isentropic expansion) for the high-pressure hydrogen release, namely the release mass flow rate, as shown in Supplementary Data Fig. S3, is considered as the source of the current calculation. The release mass flow rate of ideal gas is obtained from the choked flow Eq. (22). Meanwhile, the mass flow rate of real gas that is digitized from the published results [26], as well as the corresponding temperature and pressure can be seen in Supplementary Data Fig. S3.

The blowdown lasts dozens of seconds, however, the mass flow rate decays exponentially. Therefore, the main difference of mass release exists during the first 20 s with the deviation of

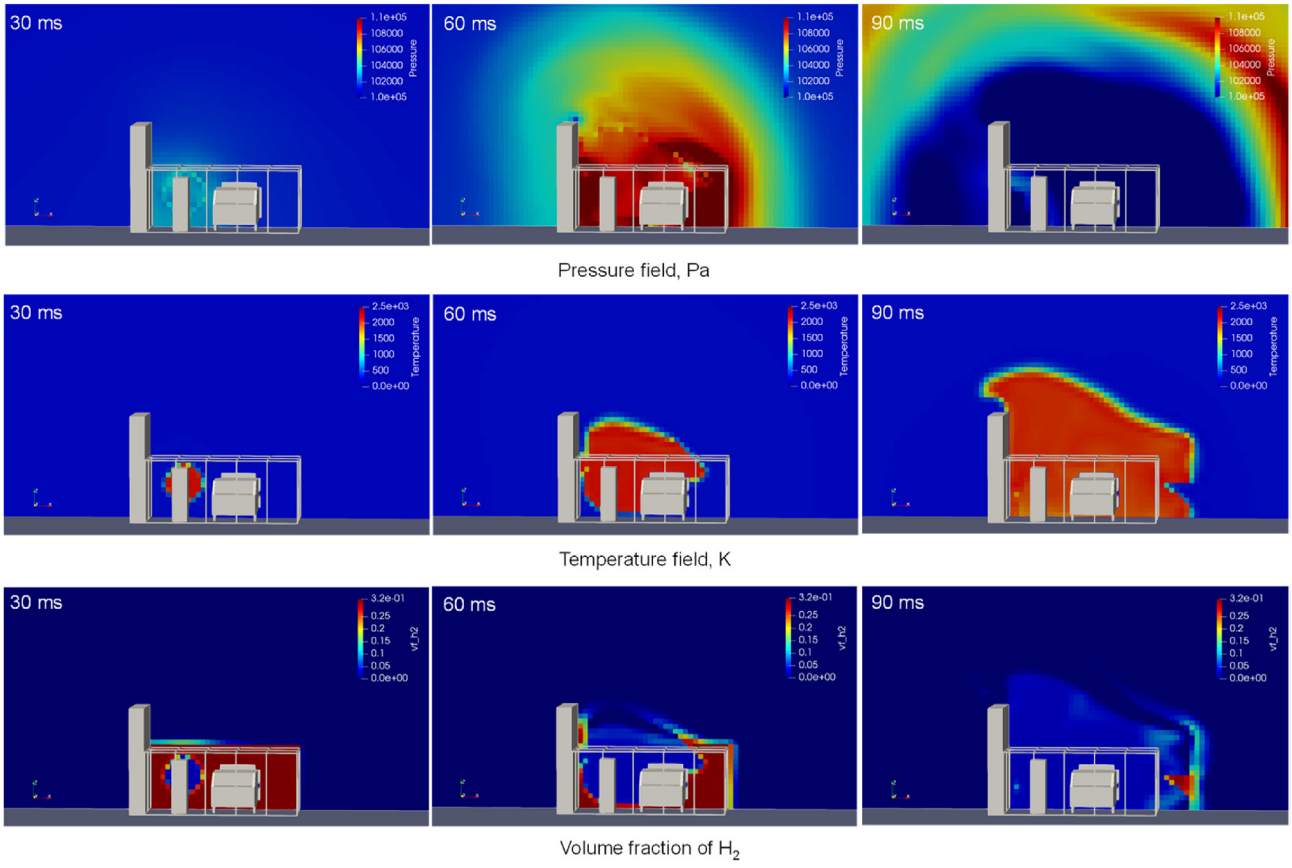

Fig. 7 – Pressure and temperature fields, and H_2 volume fraction of the slice crossing the ignition position at the time of 30 ms, 60 ms, 90 ms after ignition.

about 20%. As we know, the ideal gas mass release ignores the volume taken up by the ideal gas molecules and the attracting or repelling force between gas molecules (van der Waals force), which leads to the increase of the mass flow rate comparing with real gas. The real gas state equations for hydrogen based on Leachman's NIST model and a modified van der Waals model are implemented in GASFLOW [25], and are planted to convert it in the parallel computing version GASFLOW-MPI.

Fig. 8 demonstrates the evolutions of hydrogen concentration and velocity magnitude field of jet trial with the standard $k \quad \varepsilon$ turbulence model, Zimont turbulence burning velocity correlation and ideal gas release injection. During the H_2 dispersion after release but before combustion, the hydrogen concentration in the zone around the release location increases to the requirement of burnable cloud. The mixtures become quite reactive quickly. The turbulent flow disperses the hydrogen continuously into the air, especially into the left side ahead the vehicle. The H_2 concentration becomes lean rapidly due to the combustion in the burned zone ahead the engine bay, thereafter, the continuous H_2 injection leads to the H_2 rich again. Concerning the velocity field, we plot the velocity magnitude in both H_2 dispersion and combustion periods in the range [0, 1000] cm/s (select the range is to get a good image contrast). It can be seen in the Supplementary Data Fig. S4 that the velocity around and downward the jet is as large as a supersonic flow. The Froude number, which illustrates the ratio of momentum to buoyancy forces $Fr = \frac{u}{\sqrt{gd\frac{(\rho_{\infty} \quad \rho)}{\rho}}}$ [16,18], is easily getting over 1000 downwards the nozzle (which means the momentum dominates the hydrogen dispersion) and over 10 (which means both the momentum and buoyancy influence the dispersion) in the most experimental area due to the high jet velocity. In the dispersion phase, the H_2 distribution is consistent with the velocity field. The velocity increases rapidly and immediately following combustion, so that a large zone with high turbulence forms.

GASFLOW-MPI can evaluate the risk of the combustion sub-regimes in case of an accidental ignition in the H_2-air cloud. The global hydrogen concentration and mass over time with different threshold in a user specified computational sub-domain of interest (so-called room), can be computed by summing over all cells. Fig. 9 (left) depicts two curves of the average hydrogen concentration in room - 'engine bay' and the local hydrogen concentration at ignitor position. The

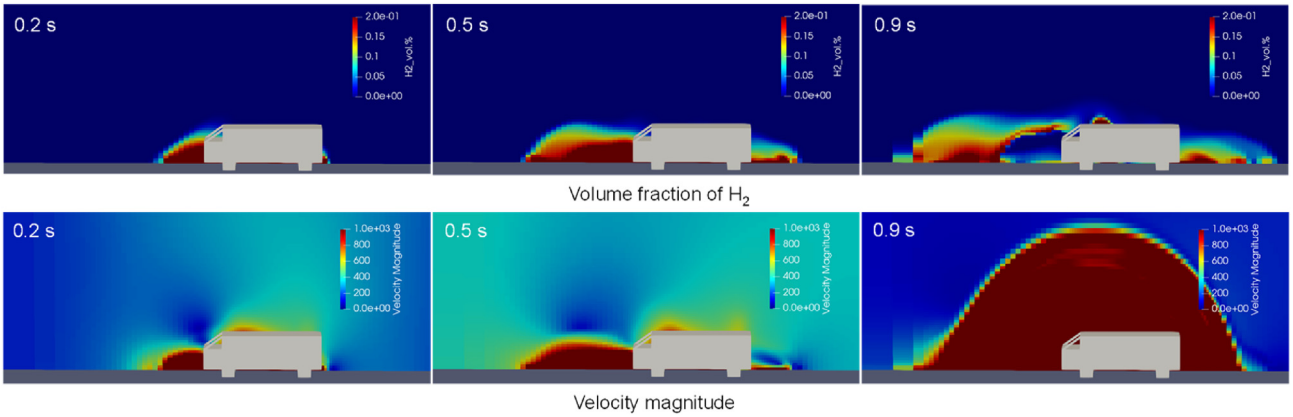

Fig. 8 – Development of hydrogen volume fraction (top subfigures) and velocity field (magnitude, bottom subfigures) of jet trial with the standard $k \quad \varepsilon$ turbulence model, Zimont turbulence burning velocity correlation and ideal gas release injection: from the left to right column at 0.2 s, 0.5 s (H_2 dispersion), 0.9 s (H_2 combustion) respectively on the y-z slice of x = 2.7 m the position of high-pressure H_2 injection.

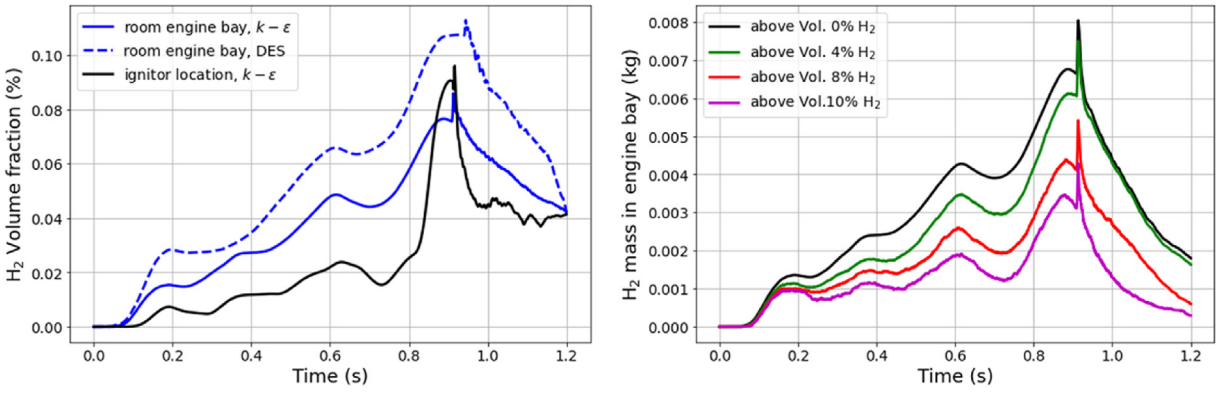

Fig. 9 – History of average hydrogen volume fraction in room engine bay during the dispersion and combustion process (left), and development of hydrogen mass of the cloud above specific hydrogen concentrations in room engine bay (right).

room engine bay, as seen in Fig. 1, refers to the ignition zone half-closed by the walls (only the bottom is open). It can be seen that the evolutions are separated into two phases - the H_2 dispersion and combustion. During the dispersion phase, the H_2 volume fraction increases gradually over time since the turbulence mixing with hydrogen continuously dilutes the air in the engine bay. Meanwhile, the H_2 concentration decreases quickly during the combustion phase even though the H_2 release is continuous. Actually, the ignition is triggered at the time of 0.7 s, the H_2 concentration at the spark position is however not sufficient to produce a propagating flame. The hydrogen concentration is too lean and outside the flammability range at this moment, however 0.1–0.2 s later the H_2 is burnable.

The hydrogen masses in the engine bay give additional insight during H_2 dispersion and combustion, as shown in Fig. 9 (right). The hydrogen mass is plotted over time that is above four given specific concentration thresholds. The black curve indicates the growth and decay of the total H_2 mass in the defined room, while the green curve shows the H_2 mass with the concentration above 4 vol% for instances, and so on. The green curve depicts the above 80% H_2 mass disperses in the burnable H_2 cloud above 4 vol% and the purple curve indicates about half H_2 mass distributes in the cloud above

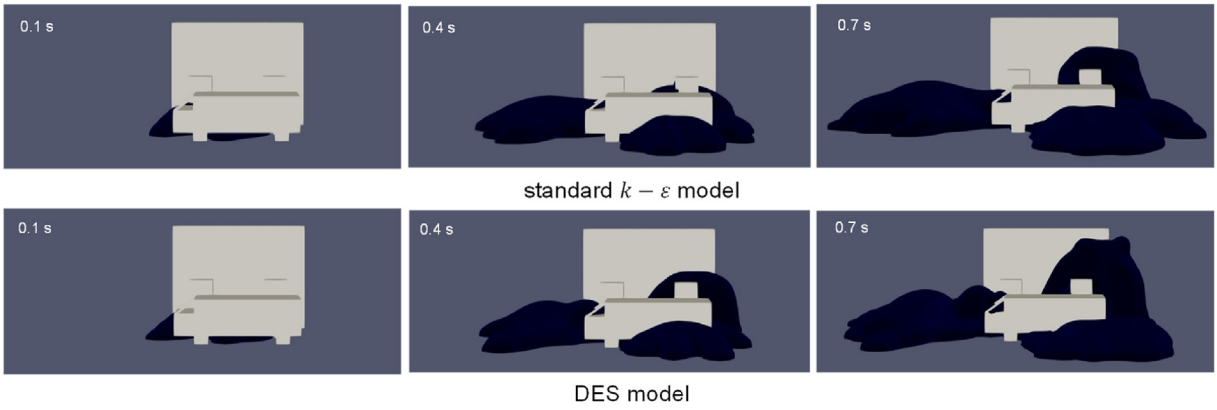

Fig. 10 – Shape and size of burnable H_2 cloud at different time 0.1 s, 0.4 s, 0.7 s: top, standard k ε model and bottom, DES model.

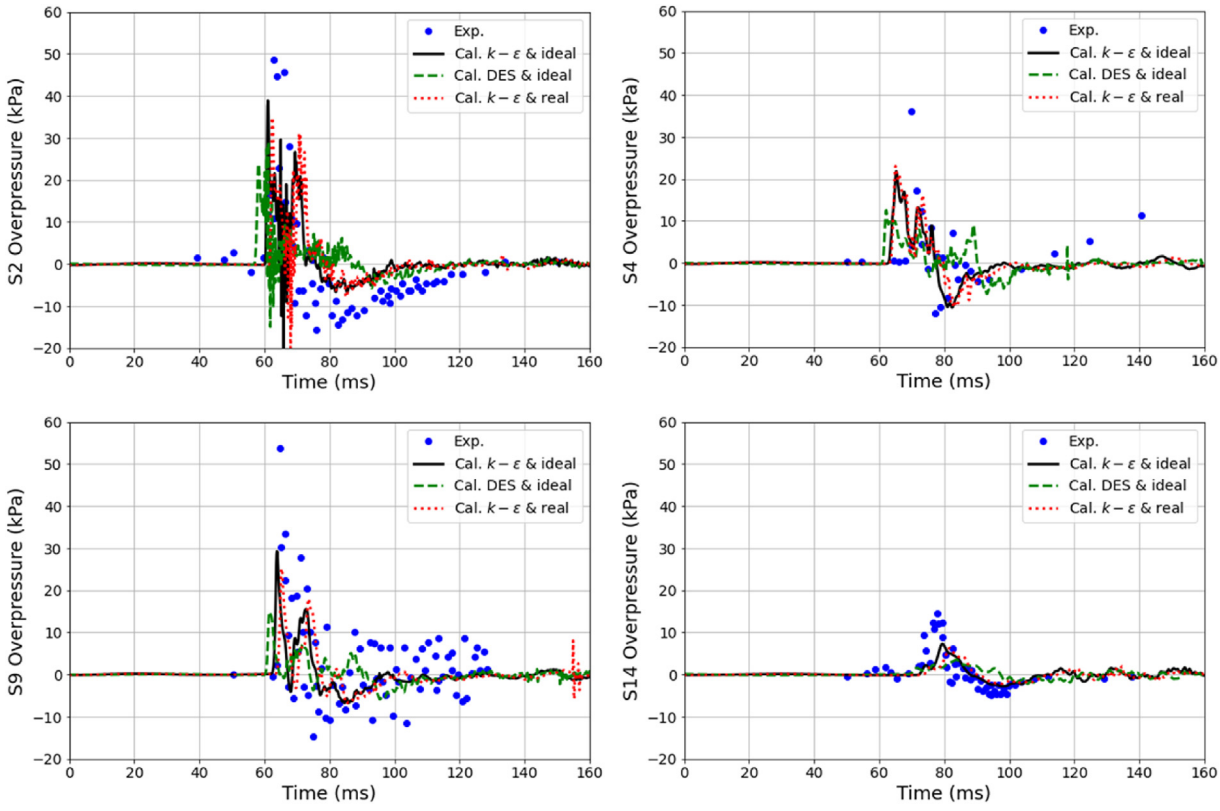

Fig. 11 – Overpressure comparison with various turbulence models and release modes.

Fig. 12 – Temperature distribution (vertical slice crossing the jet nozzle), contour (T = 1000 K) and the photo frame [21] after ignition ~ 80 ms

10 vol%, which may lead to a fast deflagration. The volume of burnable hydrogen-air mixture above the specified level (4, 8, and 10 vol% H_2) of hydrogen concentration is shown in Supplementary Data Fig. S5 as well, which indicates the similar evolutions of burnable volumes during the dispersion and combustion in the room engine bay.

For the sake of investigating the turbulence model effect on the dispersion process, the simulations are repeated with the standard k ε and Detached Eddy Simulation (DES) models by GASFLOW-MPI. Comparison shows some differences of local flow variables, as the hydrogen volume fraction in room engine bay shown in Fig. 9 (left), but the global properties of average hydrogen concentration, as well as the shape and volume of the burnable cloud (H_2 4–75 vol%) are similar, as seen in Fig. 10. The minor difference in the comparison indicates the transient hydrogen dispersion depicted with both turbulence model can provide a reliable evaluation. The diffusion with DES model is slightly more intensive than with the k-ε model since the mesh causes a relative high turbulence length, thus further leads to a high turbulence viscosity. Furthermore, Fig. 10 illustrates the high-pressure jet with a small amount H_2 release still can generate a comparable hydrogen cloud size and result in a larger overpressure comparing with the consequence of premixed trial.

In order to evaluate the combustion further, two turbulence models together with two hydrogen release modes (ideal and real gas), are involved to analyze the overpressure. Numerical simulations are carried out with the real/ideal gas release with the same sparking timing and duration. For the purpose of brevity, the simulation results for representative pressure gauges S2 (under the mock-up vehicle), S4 (mounted on the confining wall), S9 (mounted on the dispenser), and S14 (outside the vehicle) are presented in Fig. 11. In general, these are no significant difference in the comparisons of overpressure. These three calculations have similar trend keeping accordance with the experimental data. Comparing the case of ideal gas with k ε model, the case of real gas has smaller peak overpressure and slightly delay, because the injection mass flow rate is smaller, as seen in Supplementary Data Fig. S3. The difference could be larger when the injection last longer, resulting in a larger release mass difference. The case of DES model has smaller overpressure, though in some local space the hydrogen concentration is high, like in the room engine bay. There is no universal conclusion that indicates which model is more suitable for the present problem.

The fireball of the jet trial appeared very bright in the left side ahead the engine bay, as seen in Fig. 12. The fireball size captured by the camera in experiment is compared with the calculated temperature contour at 1000 K and the temperature distribution slice crossing the jet nozzle vertically after the ignition about 80 ms, i.e. at the moment when the maximum overpressure occurs. The fireball occurring on the left side of the vehicle is consistent with the previous analysis on the hydrogen dispersion and distribution (see the description of Figs. 8 and 10).

Conclusions

CFD tool GASFLOW-MPI is utilized to simulate the hydrogen deflagration experiments and investigate the physical models. The conclusions are summarized as follows:

GASFLOW-MPI is validated against the full-scale hydrogen refueling station deflagration experiments of H_2-air premixed cloud and high-pressure H_2 jet. The calculated overpressures and the maximum overpressures over the distance across and along the vehicle in the premixed trial agree well with the experimental data, while predictions of the jet trial are comparable with the experimental data.

Turbulent burning velocity correlations are investigated in the explosion of the premixed H_2–air cloud. The comparison shows Zimont correlation is recommended for the premixed combustion simulation of engineering full-scale H_2 refueling station. The turbulent flame speed is estimated around 50–200 m/s, increases rapidly and then decreases over the distance. The flame acceleration happens due to the turbulence enhanced by obstacles. The flammable H_2 cloud is enlarged by the push of combustion product.

Standard k ε and DES turbulence models are adopted in the analysis of the jet dispersion. The global properties of average hydrogen concentration, the shape and size of the burnable cloud are similar. The hydrogen dispersion transient computed with both turbulence models can provide a reliable basis for estimating the combustion process. Overpressure comparison between k ε and DES turbulence models with real and ideal gas sources shows no significant difference. The overpressures magnitudes are lower in the case of real gas due to the lower mass release.

Momentum dominates the hydrogen dispersion during the jet H_2 release, and a large zone with high turbulence forms after combustion. The growth and decay of the hydrogen dispersed in the engine bay shows most of H_2 is burnable and half of the mass distributes in the 10 vol% cloud, which indicates the flame could accelerate to sonic velocities or even a transition to detonation.

Concerning further model developments in GASFLOW-MPI, e.g. the liquid H_2 release in H_2 refueling station, it is interesting to find a suitable engineering approach that can model the liquid H_2 release as the compressed hydrogen is processed in the code.

Declaration of competing interest

The authors declare that they have no known competing financial interests or personal relationships that could have appeared to influence the work reported in this paper.

Acknowledgements

This work is supported by Innovations pool project 2021-2023 from Helmholtz-Gemeinschaft Forschungsbereich Energie – Programm MTET Zukunftsthema "Solarer Wasserstoff – hochrein und komprimiert"

Nomenclature

A	orifice/hole with cross section area m^2
C_{DES}	constant coefficient, 0.65
C_d	discharge coefficient, 0.9–0.97
$C_{\varepsilon 1}$	constant coefficient, 1.44
$C_{\varepsilon 2}$	constant coefficient, 1.92
C_μ	constant coefficient, 0.09
Da	Damköhler number
d	diameter of leakage nozzle/hole m
Fr	Froude number
g	gravity acceleration m/s^2
l_F	flame thickness m
l_t	turbulence length scale m
$\dot{m}$	mass flow rate kg/s
$\dot{m}_0$	initial release mass flow rate kg/s
P_{ref}	reference pressure Pa
P_u	pressure of the unburned mixture Pa
$P_{u,0}$	initial pressure of the unburned mixture Pa
P_κ	turbulence generation due to the viscous forces kg/(s^2·m)
$P_{\kappa b}$	turbulence production term due to the buoyancy kg/(s^2·m)
p	pressure Pa
p_1	high pressure of gas Pa
p_2	low pressure of gas Pa
R_{H_2}	gas constant for hydrogen, 4124 J/(kg·K)
Sc_t	turbulent Schmidt number
S_L	laminar flame speed m/s
$S_{L,ref}$	reference laminar flame speed m/s
S_T	turbulent flame speed m/s
$S_{\tilde{\xi}}$	source term of reaction progress variable $\tilde{\xi}$ equation 1/s
T	temperature K
T_{ref}	reference temperature K
T_u	temperature of the unburned mixture K
t	time s
u	velocity vector m/s
u'_t	turbulent velocity fluctuation m/s
V	volume of storage tank m^3
$\boldsymbol{x}$	location vector m
Y	mass fraction of the species
Δx	mesh cell length cm

Greek symbols

α	thermal diffusivity m^2/s
α_u	thermal diffusivity of the unburned mixture m^2/s
$\alpha_{u,0}$	initial thermal diffusivity of the unburned mixture m^2/s
γ	ratio of specific heats, 1.41
Δ_{max}	maximum cut-off scale of grid cells in x, y, z coordinates m
ε	turbulent dissipation rate m^2/s^3
κ	turbulent kinetic energy m^2/s^2
μ	dynamic viscosity Pa·s
μ_t	turbulent dynamic viscosity Pa·s
$\tilde{\xi}$	reaction progress variable
ρ	density kg/m^3
ρ_1	density of the high-pressure gas kg/m^3
ρ_2	density of the low-pressure gas kg/m^3
ρ_u	density of unburnt mixture kg/m^3
ρ_∞	ambient density kg/m^3
σ_b	constant coefficient, 0.7
σ_ε	constant coefficient, 1.3
σ_κ	constant coefficient, 1.0
τ_c	chemical time scale s
τ_t	turbulent integral time scale s
ϕ	equivalence ratio

REFERENCES

[1] Bentaib A, Chaumeix N. SARNET H2 combustion benchmark diluent effect on flame propagation blind phase results. France: Technology Report, IRSN; 2012.

[2] Bentaib A, Bleyer A, Meynet N, Chaumeix N, Schramm B, H öhne M, Kostka P, Movahed M, Worapittayaporn S, Brähler T, Seok-Kang H, Povilaitis M, Kljenak I, Sathiah P. SARNET hydrogen deflagration benchmarks: main outcomes and conclusions. Ann Nucl Energy 2014;74:143–52.

[3] Breitung W, Halmer G, Kuznetsov M, Xiao J. Analysis of transient supersonic hydrogen release, dispersion and combustion. Int J Hydrogen Energy 2018;44(17):9089–99.

[4] Burke EM, Güthe F, Monaghan RF. A comparison of turbulent flame speed correlations for hydrocarbon fuels at elevated pressures. In: Turbo expo: power for land, sea, and air, vol. 49767. American Society of Mechanical Engineers; 2016, June. V04BT04A043.

[5] Cheng Z, Agranat VM, Tchouvelev AV, Houf WG, Zhubrin SV. PRD hydrogen release and dispersion, a comparison of CFD results obtained from using ideal and real gas law properties. In: HYSAFE ICHS international conference on hydrogen safety; 2005, September. p. 8–10. Paper 110090. Pisa, Italy.

[6] Gerke U, Boulouchos K. Three-dimensional computational fluid dynamics simulation of hydrogen engines using a turbulent flame speed closure combustion model. Int J Engine Res 2012;13(5):464–81.
[7] Halouane Y, Dehbi A. CFD simulations of premixed hydrogen combustion using the eddy dissipation and the turbulent flame closure models. Int J Hydrogen Energy 2017;42(34):21990–2004.
[9] Launder BE, Rodi W. The turbulent wall jet measurements and modeling. Annu Rev Fluid Mech 1983;15(1):429–59.
[10] Magnussen BF, Hjertager BH. On mathematical modeling of turbulent combustion with special emphasis on soot formation and combustion. In: Symposium (international) on combustion, vol. 16. Elsevier; 1977, January. p. 719–29. No. 1.
[11] Makarov D, Verbecke F, Molkov V, Roe O, Skotenne M, Kotchourko A, Lelyakin A, Yanez J, Hansen O, Middha P, Ledin S, Baraldi D, Heitsch M, Efimenko A, Gavrikov A. An inter-comparison exercise on CFD model capabilities to predict a hydrogen explosion in a simulated vehicle refuelling environment. Int J Hydrogen Energy 2009;34(6):2800–14.
[12] Metghalchi M, Keck JC. Burning velocities of mixtures of air with methanol, isooctane, and indolene at high pressure and temperature. Combust Flame 1982;48:191–210.
[13] Pagliaro M, Iulianelli A. Hydrogen refueling stations: safety and sustainability. Gen Chem 2020;6(1):190029.
[14] Peters N. The turbulent burning velocity for large-scale and small-scale turbulence. J Fluid Mech 1999;384:107–32.
[15] Povilaitis M, Jaseliūnaitė J. Simulation of hydrogen-air-diluents mixture combustion in an acceleration tube with FlameFoam solver. Energies 2021;14(17):5504.
[16] Qian JY, Li XJ, Gao ZX, Jin ZJ. A numerical study of hydrogen leakage and diffusion in a hydrogen refueling station. Int J Hydrogen Energy 2020;45(28):14428–39.
[17] Rose P. Modeling a potential hydrogen refueling station network for fuel cell heavy-duty vehicles in Germany in 2050. PhD dissertation. Germany: Karlsruhe Institute of Technology (KIT); 2020.
[18] Schefer RW, Houf WG, Williams TC. Investigation of small-scale unintended releases of hydrogen: momentum-dominated regime. Int J Hydrogen Energy 2008;33(21):6373–84.
[19] Sherman MP, Tieszen SR, Benedick WB. FLAME facility: the effect of obstacles and transverse venting on flame acceleration and transition on detonation for hydrogen-air mixtures at large scale (No. NUREG/CR-5275; SAND-85-1264). Nuclear Regulatory Commission, Washington, DC (USA). Albuquerque, NM (USA): Div. of Systems Research; Sandia National Labs; 1989.
[20] Shirvill LC, Royle M, Roberts TA. Hydrogen releases ignited in a simulated vehicle refuelling environment. In: International conference on hydrogen safety. Spain: S. Sebastian; 2007, September. p. 11–3.
[21] Shirvill LC, Roberts TA, Royle M, Willoughby DB, Gautier T. Safety studies on high-pressure hydrogen vehicle refuelling stations: releases into a simulated high-pressure dispensing area. Int J Hydrogen Energy 2012;37(8):6949–64.
[22] Smith LM, Woodruff SL. Renormalization-group analysis of turbulence. Annu Rev Fluid Mech 1998;30(1):275–310.
[23] Takeno K, Okabayashi K, Kouchi A, Nonaka T, Hashiguchi K, Chitose K. Dispersion and explosion field tests for 40 MPa pressurized hydrogen. Int J Hydrogen Energy 2007;32(13):2144–53.
[24] Tanaka T, Azuma T, Evans JA, Cronin PM, Johnson DM, Cleaver RP. Experimental study on hydrogen explosions in a full-scale hydrogen filling station model. Int J Hydrogen Energy 2007;32(13):2162–70.
[25] Travis JR, Koch DP. GASFLOW analysis for the HySIM hydrogen refueling benchmark. J Energy Storage 2015;2:47–53.
[26] Wen JX, Rao VM, Tam VHY. Numerical study of hydrogen explosions in a refuelling environment and in a model storage room. Int J Hydrogen Energy 2010;35(1):385–94.
[27] Xiao J, Travis JR, Kuznetsov M. Numerical investigations of heat losses to confinement structures from hydrogen-air turbulent flames in ENACCEF facility. Int J Hydrogen Energy 2015;40(38):13106–20.
[28] Xiao J, Travis JR, Royl P, Necker G, Svishchev A, Jordan T. Three-dimensional all-speed CFD code for safety analysis of nuclear reactor containment: status of GASFLOW parallelization, model development, validation and application. Nucl Eng Des 2016a;301:290–310.
[29] Xiao J, Travis JR, Royl P, Necker G, Svishchev A, Jordan T. In: GASFLOW-MPI: a scalable computational fluid dynamics code for gases, aerosols and combustion", vol. 1. Germany: Karlsruhe Institute of Technology (KIT); 2016b. Theory and Computational Model (Revision 1.0), ISBN 978-3-7315-0448-1.
[30] Xiao J, Travis JR, Royl P, Necker G, Svishchev A, Jordan T. In: GASFLOW-MPI: a scalable computational fluid dynamics code for gases, aerosols and combustion", vol. 2. Germany: Karlsruhe Institute of Technology (KIT); 2016c. Users' Manual (Revision 1.0), ISBN 978-3-7315-0449-8.
[31] Xiao J, Breitung W, Kuznetsov M, Zhang H, Travis JR, Redlinger R, Jordan T. GASFLOW-MPI: a new 3-D parallel all-speed CFD code for turbulent dispersion and combustion simulations: Part I: models, verification and validation. Int J Hydrogen Energy 2017;42(12):8346–68.
[33] Zimont VL, Mesheriakov EA. A model of combustion of partially premixed gases. In: Structure of gas flames. Proceedings of international colloquium. Part II; 1988. p. 35–43. Novosibirsk, Russia.
[34] Zimont VL. Gas premixed combustion at high turbulence. Turbulent flame closure combustion model. Exp Therm Fluid Sci 2000;21(1–3):179–86.
[35] Zhang H, Li Y, Xiao J, Jordan T. Detached Eddy Simulation of hydrogen turbulent dispersion in nuclear containment compartment using GASFLOW-MPI. Int J Hydrogen Energy 2018;43(29):13659–75.
[36] Zur Loye AO, Bracco FV. Two-dimensional visualization of premixed-charge flame structure in an IC engine. Princeton, NJ (USA): Princeton University; 1987.